AIAA-2014-3341

7th AIAA Theoretical Fluid Mechanics Conference, 16-20 June 2014, Atlanta, GA

Study of unsteady shock motion in shock/turbulence interaction

Palash Sashittal*, Yogesh Prasaad M S† and Krishnendu Sinha‡

Indian Institute of Technology Bombay, Mumbai, Maharashtra, 400 076, India

Johan Larsson§

University of Maryland, College Park, Maryland, 20742, USA

The interaction of turbulence with a shock wave is common in high speed flow applications. The shock wave distorts upon interaction and an unsteadiness is observed in the flow. The amount of distortion depends on the intensity of the incoming fluctuations and at very high intensities, the shock wave cannot maintain its profile and instead develops holes. This rather interesting feature has been observed in direct numerical simulations (DNS) of shock-turbulence interaction.

In the present study, we investigate whether analogous "shock holes" can be created in a one-dimensional setting, i.e., where the incoming waves are perfectly planar and normal to the shock. The results are used to draw inferences about the fully three-dimensional physics, specifically whether certain aspects of the shock-turbulence interaction process are inherently multi-dimensional phenomena.

Nomenclature

a	Speed of sound
k	Wavenumber
p	Pressure
t	Time
u, v	Velocity in streamwise and transverse direction
x, y	Streamwise and transverse directions

Subscripts

d	Downstream of the shock
in	At the inflow
rms	root mean square
s	At the shock
sp	Sponge
u	Upstream of the shock

Conventions

$\bar{}$	Reynolds averaging
$'$	Reynolds fluctuations

Symbols

*Undergraduate Student, Department of Aerospace Engineering, Indian Institute of Technology Bombay

†Graduate Student, Department of Aerospace Engineering, Indian Institute of Technology Bombay, and AIAA Student Member.

‡Associate Professor, Department of Aerospace Engineering, Indian Institute of Technology Bombay, and AIAA Senior Member.

§Assistant Professor, Department of Mechanical Engineering, University of Maryland, and AIAA Member.

ω	Wave frequency
ρ	Density
θ	Strength of shock
τ	Time lag

I. Introduction

SHOCK-turbulence interactions are common in high speed flows, and the dynamics of these interaction are widely studied for better design and optimization of aerospace vehicles. The canonical shock-turbulence interaction problem is that of isotropic turbulence passing through a nominally normal shock wave. This problem rarely occurs in practice, but is studied as a building-block flow that isolates the key physics. The more practically-relevant problem is that of the interaction between a shock and a turbulent boundary layer, in which the unsteady shock motion may cause (or be caused by) oscillatory flow separation. The resulting oscillatory nature of the shock/boundary-layer interaction causes large pressure and heating loads.

The canonical shock-turbulence interaction problem offers a "clean" environment in which to study shock motion, since it isolates the shock motion induced by the turbulence itself. One of the more interesting aspects of canonical shock-turbulence interaction is that the turbulence may locally extinguish the shock and create a "shock hole", where the local compression is perfectly smooth. This has been found in two-fluid experiments[1] as well as in single-fluid direct numerical simulations (DNS).[2,3,4] A natural question to ask is how these "shock holes" are created? While they are seen quite readily in DNS, at least for turbulent Mach numbers M_t greater than about $0.6(M-1)$[4,5] [note that this criterion is based on the definition $M_t^2 = \overline{u_k' u_k'}/a^2$, and thus the equivalent one-dimensional criterion would be $u'/a \gtrsim 0.35(M-1)$], it is difficult or even impossible to extract the cause-and-effect relationships in data from a DNS.

In the present study we take a different approach, and study purely one-dimensional interactions between a shock wave and incoming disturbances. Those aspects of the interaction dynamics that can be successfully replicated are then plausibly caused by one-dimensional physics embedded in the fully three-dimensional shock-turbulence interaction, whereas those aspects that cannot be replicated are plausibly inherently caused by multi-dimensional processes (e.g., non-orthogonality between streamlines and the shock surface). The amplitude of the incoming disturbances is increased with the intention of breaking the shock (i.e., creating "shock holes"). The present study is related to that of Zank *et al.*,[6] which found that incoming fluctuations could easily break a shock in the Burgers' equation.

II. Methodology

The one-dimensional Euler equations are solved for a perfect gas with ratio of specific heats $\gamma = 1.4$ using a third order accurate weighted essentially non-oscillatory (WENO) numerical scheme with Roe flux splitting. The system is integrated in time using a fourth order accurate Runge-Kutta method. The resolved portion of the computational domain (i.e., excluding the sponge region) is 4π in length with uniform grid spacing.

II.A. Inflow conditions

The mean flow upstream of the shock (subscript "u") is taken as

$$(\overline{\rho}_u, \overline{u}_u, \overline{p}_u) = (1.0, 1.5, 0.714286)\,,$$

which corresponds to a Mach $M = 1.5$ flow. Note that all quantities in this paper are normalized by the upstream density and speed-of-sound. Initial downstream mean quantities are obtained from the normal shock relations. Sinusoidal fluctuations corresponding to acoustic, vorticity or entropy modes, or a linear combination of these modes, are superposed at the inlet. Acoustic waves with wave speed of $u + a$ are referred to as right moving acoustic waves and with wave speed of $u - a$ as left moving acoustic waves. The transverse momentum equation (y direction) of Euler equations is also solved with the mean upstream transverse velocity being zero (i.e. $\overline{v}_u = 0$). Thus the complete inflow conditions are

$$p = \overline{p}_u + \overline{p}_u \sum_{k=0}^{\infty} A_{p^+} e^{-ik(\overline{u}_u + a_u)t} + \overline{p}_u \sum_{k=0}^{\infty} A_{p^-} e^{-ik(\overline{u}_u - a_u)t} \tag{1a}$$

$$\rho = \overline{\rho}_u + \overline{\rho}_u \sum_{k=0}^{\infty} A_e e^{-ik\overline{u}_u t} + \overline{\rho}_u \sum_{k=0}^{\infty} \frac{A_{p^+}}{\gamma} e^{-ik(\overline{u}_u + a_u)t} + \overline{\rho}_u \sum_{k=0}^{\infty} \frac{A_{p^-}}{\gamma} e^{-ik(\overline{u}_u - a_u)t} \tag{1b}$$

$$u = \overline{u}_u + \overline{u}_u \sum_{k=0}^{\infty} \frac{A_{p^+}}{\gamma M} e^{-ik(\overline{u}_u + a_u)t} - \overline{u}_u \sum_{k=0}^{\infty} \frac{A_{p^-}}{\gamma M} e^{-ik(\overline{u}_u - a_u)t} \tag{1c}$$

$$v = -\overline{u}_u \sum_{k=0}^{\infty} A_v e^{-ik\overline{u}_u t} \tag{1d}$$

where, A_{p^+}, A_{p^-}, A_v and A_e are the amplitudes of right moving acoustic wave fluctuations, left moving acoustic wave fluctuations, vortical wave fluctuations and entropic wave fluctuations, respectively. Note that the amplitude is a function of wavenumber and also vary accordingly. For cases with broadband inflow conditions, meant to mimic upstream turbulence, we use the truncated von Karman spectrum given by[7]

$$E(k) \sim \frac{(k/k_0)^2}{k_0 \left((k/k_0)^2 + 5/6\right)^{11/6}} \quad \text{for } k/k_0 < 2.5\,. \tag{2}$$

II.B. Outflow conditions

The resolved (useful) part of the computational domain ends at $x = 4\pi$. Beyond this, a sponge region is appended to gently damp disturbances before reaching the outlet, thus minimizing spurious reflections. In the sponge layer, source terms of form

$$-\sigma_0 \left(\frac{x - x_{sp}}{L_{sp}}\right)^2 (q - q^*) \tag{3}$$

are added to each equation, where q denotes the particular conserved variable in each equation, σ_0, x_{sp} and L_{sp} denote the strength coefficient, beginning and length of the sponge, respectively. The target state q^* for all quantities except pressure, is taken as the post shock state obtained from Rankine-Hugoniot (R-H) shock relations. The target state for pressure is taken as the back pressure specified at the outlet. The shock wave experiences a different back pressure than the back pressure obtained from Rankine-Hugoniot (R-H) shock relations due to the fluctuations in the flow-field and thus tend to drift in the domain. The back pressure is varied case by case to keep the shock drift always less than 1% of the mean upstream velocity (i.e.) $\overline{u}_s/\overline{u}_u < 0.01$. Variation of normalized shock position in time are shown in figure 1 where it is observed that the mean shock drift velocity after the initial transient is found to be within the error limits.

II.C. Grid convergence

A combination of acoustic, vorticity and entropy with 10% amplitude each has been tested for grid convergence. In one-dimensional framework, the difference in pressure variance normalized by the pressure variance at the inflow ($\overline{p'^2}/\overline{p'^2_{in}}$) with different grid spacings has been used as the error metric for grid convergence. The error in normalized pressure variance between two finest grids considered is less than 3% and thus the solution is assumed to be grid converged (shown in figure 2). Similarly, broadband of right moving acoustic waves with upstream intensity ($u_{rms}/\overline{u}_u$) of 0.2 has been considered for grid convergence study for the broadband cases. The solution with grid spacing of $\pi/100$ is found to be grid converged.

II.D. Sponge convergence

Sponge region added to the useful part of the computational domain must be of sufficient length and strength to reduce spurious reflections from the outflow boundary. There are two kinds of reflections that enter the

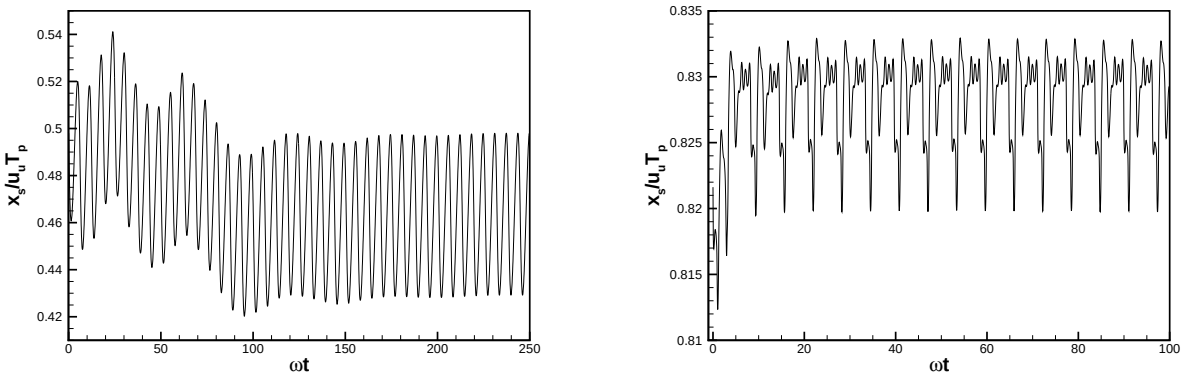

Figure 1. Normalized shock position for the (a) entropy wave of 50% amplitude density fluctuations, (b) broadband acoustic waves with upstream $u_{rms}/\overline{u}_u$ of 0.1. Time is normalized with characteristic frequency(ω) of the respective wave and shock location is normalized by upstream mean velocity $\overline{u}_u$ and time period(T_p) of the incoming fluctuations.

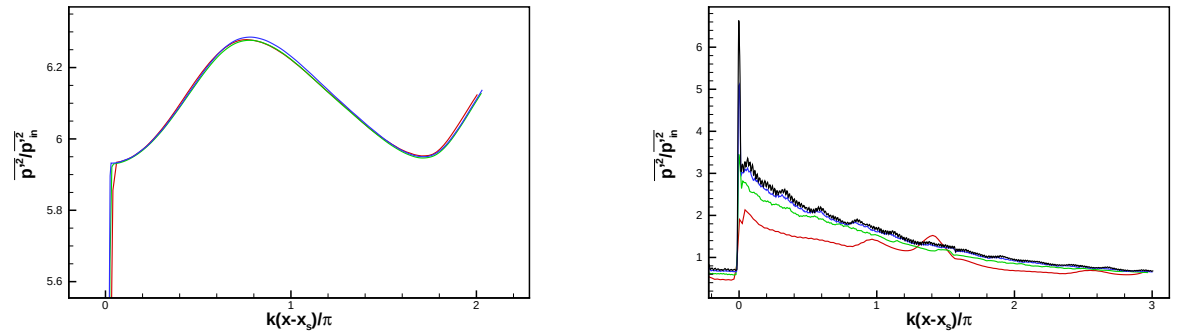

Figure 2. Stream-wise variation of normalized pressure variance for different grid sizes in (a) 1D combination of acoustic-vorticity-entropy modes each of 10% amplitude, (b) Acoustic broadband case with upstream intensity ($u_{rms}/\overline{u}_u$) of 0.1. $\Delta x = \pi/50$ (Red), $\Delta x = \pi/100$ (Green), $\Delta x = \pi/200$ (Blue), $\Delta x = \pi/400$ (Black).

useful domain, which are reflections from the outflow boundary and reflections from inside the sponge. To analyze the sponge, the approximate scalar equation

$$\frac{\partial q'}{\partial t} + \lambda \frac{\partial q'}{\partial x} = -\sigma q' \tag{4}$$

is considered, where σ is assumed constant, $q' = q - q^*$ is the deviation of the solution from the target state, and λ is the propagation velocity (either $\overline{u}_d$ or $\overline{u}_d \pm a_d$ depending on the wave type).

Making the ansatz $q' = e^{i(kx-\omega t)}$ where ω is taken as a real-valued frequency and k is taken as a complex wavenumber (i.e., considering a spatially evolving problem), the dispersion relation $-i\omega + ik_r\lambda - k_i\lambda + \sigma = 0$ is obtained, which implies $\omega = k_r\lambda$ and $k_i = \sigma/\lambda$. Thus the damping of the solution at the end of the domain scales with $\alpha_d = \sigma_0 L_{sp}/\lambda$, where higher values of α_d are desirable. Reflections inside the sponge occur when the damping length scale $\sim 1/k_i$ is short compared to the wave length $\sim 1/|k_r|$. Therefore, a reflection coefficient can be defined as $\alpha_r = (1/k_i)/(1/|k_r|) = |k_r|\lambda/\sigma_0$, where high values of α_r are desirable.

When assessing a sponge layer, it is important to note that the coefficients α_d and α_r are independent parameters, whereas the strength σ_0 and length L_{sp} are not.

The error metric used in grid convergence study is used also for the sponge convergence study. A grid spacing of $\pi/100$ is chosen for this test. The largest error in normalized pressure variance between sponges of two different reflection coefficients is 3% as shown in figure 3 where the reflection coefficients of one sponge are double of the other. The solution with a sponge of length $L_{sp} = 4\pi$ and strength $\sigma = 1.0$ is found to be sponge converged.

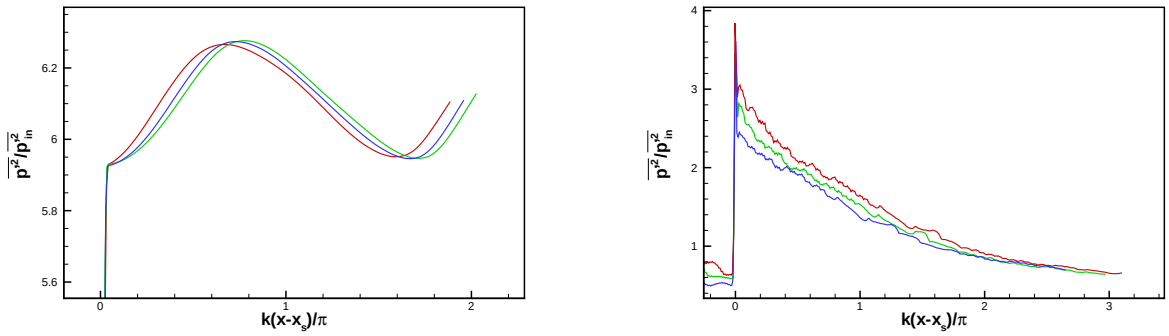

(a) (b)

Figure 3. Stream-wise variation of normalized pressure variance for different sponge sizes and strengths in (a) 1D combination of acoustic-vorticity-entropy modes each of 10% amplitude, (b) Acoustic broadband case with upstream intensity ($u_{rms}/\overline{u}_u$) of 0.1. $L_{sp} = 1\pi$, $\sigma = 2$, $\alpha_r = 1$ and $\alpha_d = 1$ (Red), $L_{sp} = 4\pi$, $\sigma = 1.0$, $\alpha_r = 2$ and $\alpha_d = 2$ (Green), $L_{sp} = 16\pi$, $\sigma = 0.5$, $\alpha_r = 4, \alpha_d = 4$ (Blue). α_r and α_d are normalized quantities.

III. Broken shock regime

In this study we attempt to break a shock in one dimensional Euler simulations. To do this we force the shock to interact with different kind of waves of varying amplitudes. Kovaznay[8] showed that small amplitude fluctuations in a compressible medium can be decomposed into three modes. These are the vorticity, entropy and acoustic modes. Interaction of any one of these modes with the shock can generate all three kind of disturbances downstream of the shock.

Vorticity mode is a solenoidal velocity field that is convected by the mean flow. It has no pressure, density or temperature fluctuations. In a one-dimensional framework, a vorticity wave will have only transverse velocity fluctuations which pass through shock without disturbing it. In such a case, the amplitude of vorticity wave does not change as it passes through the shock and no new waves are generated at the shock. The wave length of the vorticity wave decreases by a factor of $\overline{u}_d/\overline{u}_u$. Since the shock is not perturbed, this wave is not capable of breaking the shock.

Table 1. List of cases attempted to identify shock breaking phenomenon

Wave mode	Fluctuation amplitude	u_{rms}/a
Entropy single mode	10%	-
	30%	-
	50%	-
	80%	-
Right moving acoustic single mode	10%	0.071
	30%	0.214
	50%	0.357
	80%	0.571
Right moving acoustic broadband	-	0.15
	-	0.225
	-	0.3
Left moving acoustic broadband	-	0.15
	-	0.225
	-	0.3

The remaining two modes namely, entropy and acoustic modes, both perturb the shock in a one dimensional setting. Entropy wave is convected by the mean flow and has no velocity or pressure fluctuations.

It only has density and temperature fluctuations. Acoustic wave travels with the speed of sound relative to the mean flow and has isentropic pressure and density fluctuations. The velocity field for this mode is irrotational. Both single mode and broadband fluctuations of this mode are considered in an attempt to break the shock. Also, both left and right moving acoustic waves are simulated.

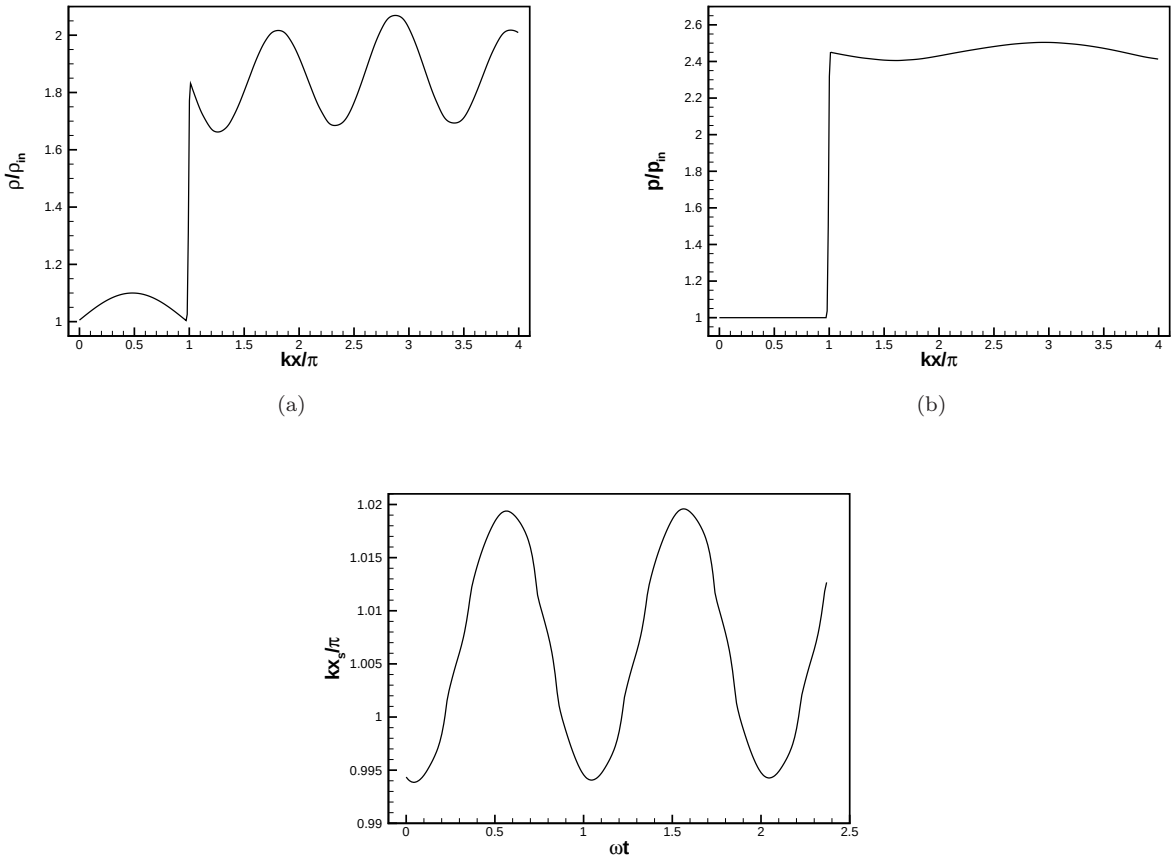

Figure 4. Instantaneous profile of streamwise variation of (a) normalized density (b) normalized pressure and (c) temporal variation of shock location (x_s) for 10% amplitude entropy wave interaction with a $M = 1.5$ shock. Distances x_s and x are normalized by upstream wavenumber k and π. Time is normalized by upstream frequency ω

Table 1 lists all the cases that were analyzed in this study. The fluctuation amplitudes are mentioned for density fluctuations for entropy waves and pressure fluctuations for right moving acoustic waves. A 10% fluctuation amplitude for entropy wave means that amplitude of upstream density fluctuations is 10% of upstream mean density. Similarly a 10% fluctuation amplitude for acoustic wave means that amplitude of upstream pressure fluctuations is 10% of upstream mean pressure. It is to be noted that entropy cases do not have any fluctuations in the streamwise velocity component. Hence u_{rms} upstream of the shock for these cases is 0.

Figures 4(a) and 4(b) show instantaneous profiles of density and pressure for a single mode 10% amplitude entropy wave passing through a $M = 1.5$ shock. The shock is placed close to $kx/\pi = 1$ and the sponge region begins at $kx/\pi = 4$. There are no pressure fluctuations upstream of the shock. An acoustic mode is generated at the shock which gives rise to sinusoidal pressure fluctuations downstream. The density fluctuations downstream however, are not perfectly sinusoidal since they have contributions from both entropy and acoustic modes which have different wavenumbers and wave speeds. Figure 4(c) shows the shock location for the same case with time. Shock location oscillates around mean location of $kx/\pi = 1.006$ and has the same time period as the upstream fluctuations.

The effect of varying density fluctuations on the shock is analyzed. The values of upstream density fluctuations considered are 30%, 50% and 80%. The corresponding $x - t$ diagrams highlighting the pressure

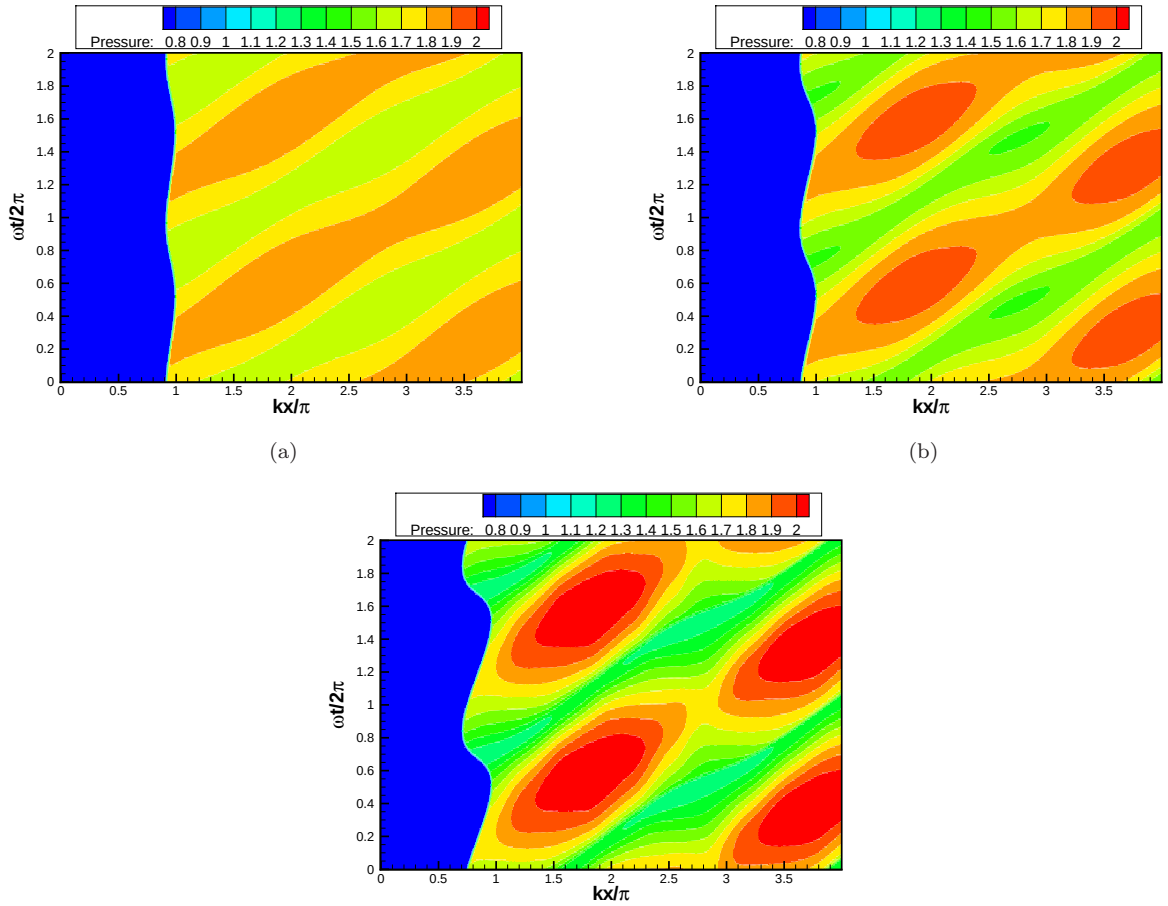

Figure 5. Pressure contours in x-t plane for entropy wave with (a) 30% amplitude in density fluctuations (b) 50% amplitude in density fluctuations (c) 80% amplitude in density fluctuations passing through a $M = 1.5$ shock

contours are shown in figure 5. The wavy vertical line close to $kx/\pi = 1$ indicating a sharp jump in pressure, represents the shock structure. The blue region upstream of the shock indicates zero pressure fluctuations. Upon increasing the magnitude of upstream density fluctuations, a clear increase in shock waviness is observed. Moreover the shock displacement at higher amplitudes takes a non-sinusoidal form as can be clearly seen in figure 5(c). The shock in spite of high upstream fluctuations seems to remain unbroken, which means that there is no time interval in which the shock gradient is replaced by a smooth compression from upstream to downstream flow.

Next, acoustic wave interaction with the shock is considered. Same conditions as the entropy case are chosen for the study. Right moving acoustic waves with pressure fluctuations of 30%, 50% and 80% are considered. Planar acoustic waves interacting with the shock, however, do not seem to induce high amplitude shock waviness as seen in figure 5(c) of the entropy case. Wave steepening is observed in these cases (for example in figure 6 (b), in the blue region). This is typical for a high amplitude non-linear wave. The compression peaks travel faster than the rarefraction minimum pressure so that over time the leading edge has a steeper slope than the trailing edge. Even for these cases the sharp jump in pressure can be easily seen in the figures. Therefore, the shock is not broken, although it appears to come close to breaking for the highest amplitude case (figure 6 (c)) for example at $\omega\tau/2\pi$ close to 0.2.

Following single mode disturbance waves, broadband perturbations of left and right moving acoustic waves were attempted to observe shock holes. The inflow is forced with superposition of acoustic waves with different wavelengths and random phase such that the velocity field satisfies the von Karman spectrum given in Eq. 2. An upstream intensity $(u_{rms}/\overline{u}_u)$ of 0.2, which corresponds to upstream $u_{rms}/a = 0.3$, was chosen for this study. This intensity is much higher than the one dimensional criterion equivalent to the one put forth in Ref. 4,5 for three dimensional flow. The pressure contours in $x - t$ plane for the broadband cases

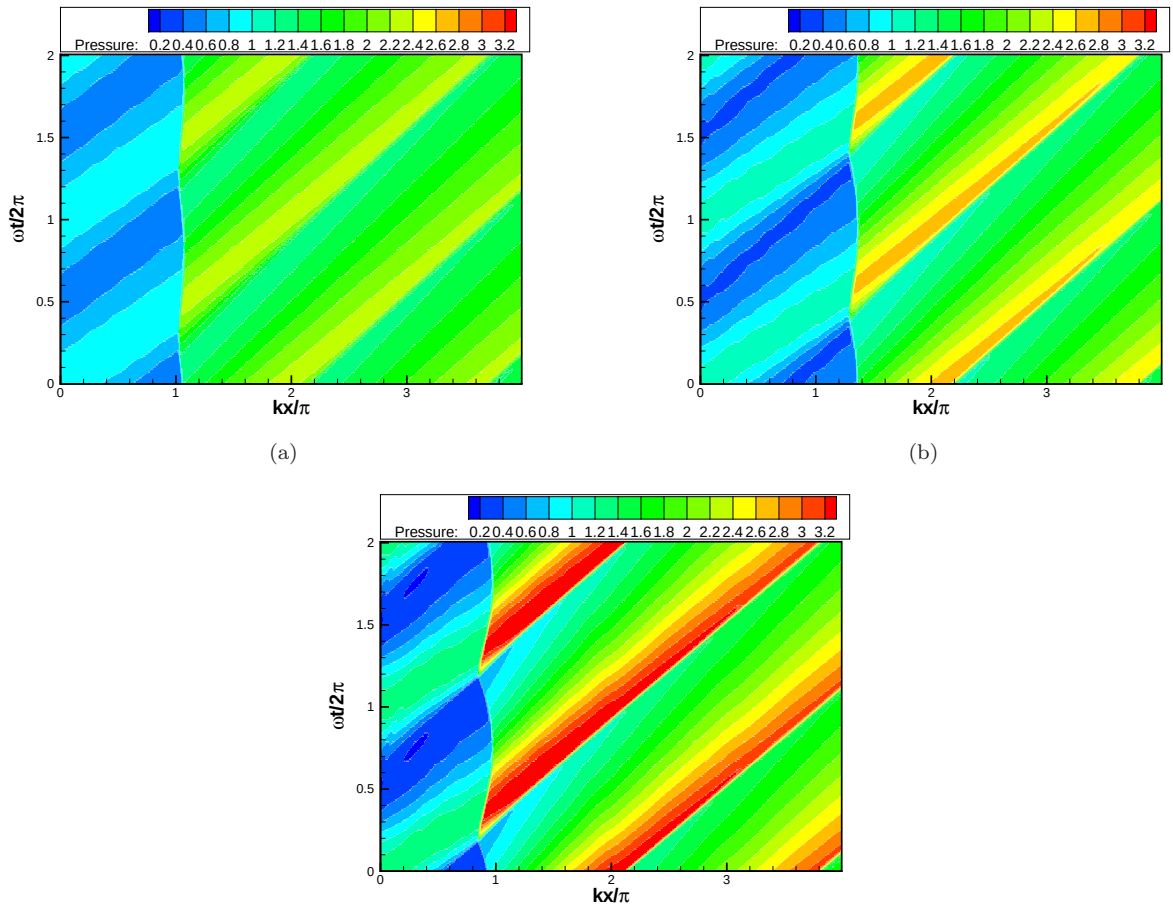

Figure 6. Pressure contours in $x-t$ plane for right moving acoustic wave (a) 30% amplitude in pressure fluctuations (b) 50% amplitude in pressure fluctuations (c) 80% amplitude in pressure fluctuations passing through a $M = 1.5$ shock

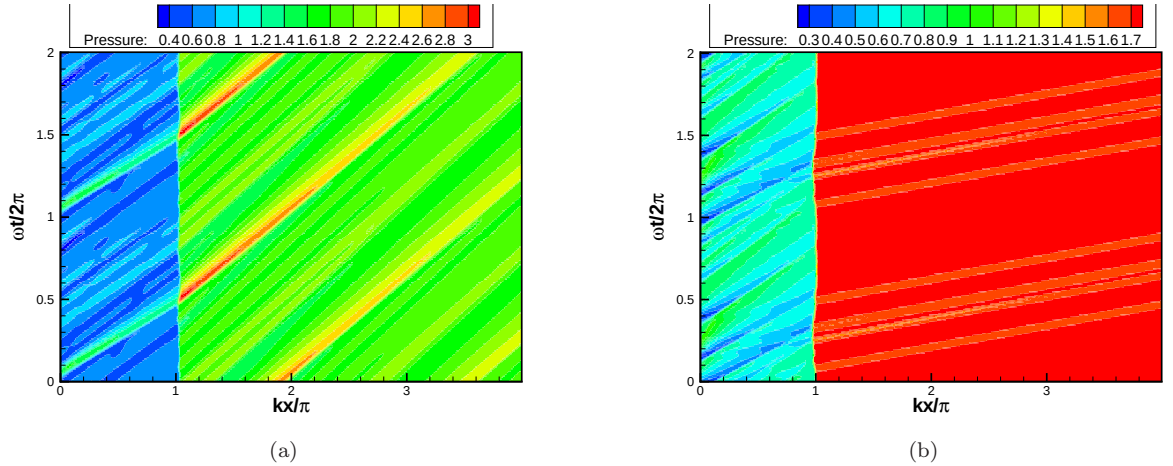

Figure 7. Pressure contours in $x-t$ plane for broadband (a) right moving acoustic waves (b) left moving acoustic waves with upstream turbulence intensity of 0.2 passing through a $M = 1.5$ shock

are shown in figure 7. It is seen that the shock is intact in all of these cases. Within the scope of this work, we can say that it is much more difficult to break the shock in a one-dimensional simulation than in a three dimensional simulation.

IV. Shock statistics

One of the objectives of this study is to investigate whether a one-dimensional model problem can be formulated to investigate the unsteady shock motion in three-dimensional shock-turbulence interaction. To do this, we try to replicate the shock statistics in a shock turbulence interaction by forcing the inflow with different kinds of fluctuations in a one dimensional framework.

Results from one-dimensional interactions of acoustic and entropy waves with a shock are compared with DNS results of isotropic turbulence interacting with a normal shock.[3] Upstream turbulence intensity of 0.16 and upstream Mach number of 1.5 is chosen. Single mode entropy, right moving acoustic and left moving acoustic waves are chosen for this study. Further, broadband right and left moving acoustic waves are also considered. We match the M_t/M ratio of all the cases considered (except the single mode entropy wave case) and compare their shock statistics. For single mode entropy wave case we take an entropy wave with 10% amplitude in density fluctuations.

Let us first define certain properties of the shock. Shock location is defined as the point where the instantaneous pressure profile crosses a pressure threshold. The pressure threshold is taken as average of the mean pressure upstream and downstream of the shock. Shock speed is time derivative of the instantaneous shock location. Shock strength (labelled as θ) is measured as the instantaneous density jump across the shock. The jumps across the shock are taken three grid points ahead and behind the instantaneous shock location. The streamwise velocity fluctuations just upstream of the shock are also measured likewise. We study the correlations between shock speed, shock strength and upstream velocity plotted against normalized time lag. For all the cases the time lag is normalized by characteristic frequency (derived from the wavelength corresponding to peak energy). Correlation coefficient is plotted as a function of the normalized time lag for the one-dimensional interactions and the DNS case. The correlation of two signals for a given time lag τ is given by,

$$\overline{fg}(\tau) = \int_0^{T_p} f(t)g(t+\tau)d\tau \tag{5}$$

where, f and g are the two signals and T_p is the time period of the signals.

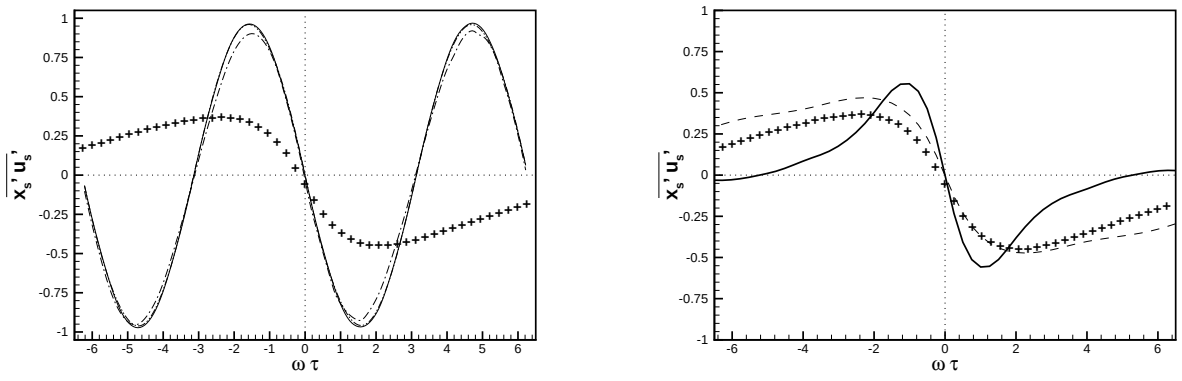

Figure 8. Correlation coefficients of $\overline{x_s' u_s'}$ for different waves (lines) compared to DNS (symbols). (a) entropy wave (Thin solid), right moving acoustic wave (DashDotDot), left moving acoustic wave (DashDot), (b) broadband of right moving acoustic waves (Thick Solid) and broadband of left moving acoustic waves (Dashed).

For the single mode cases, the velocity fluctuations upstream of the shock are sinusoidal and the shock response, as per Linear Interaction Analysis (LIA), is sinusoidal.[9] Further, the one-dimensional cases considered in this work are in the propagating regime. As a result, the upstream and downstream fluctuations, as well as the shock motion have the same time period and are in-phase. Since the shock location is the integral of shock speed, it is at $\pi/2$ phase difference with the shock speed. Therefore, the correlation of

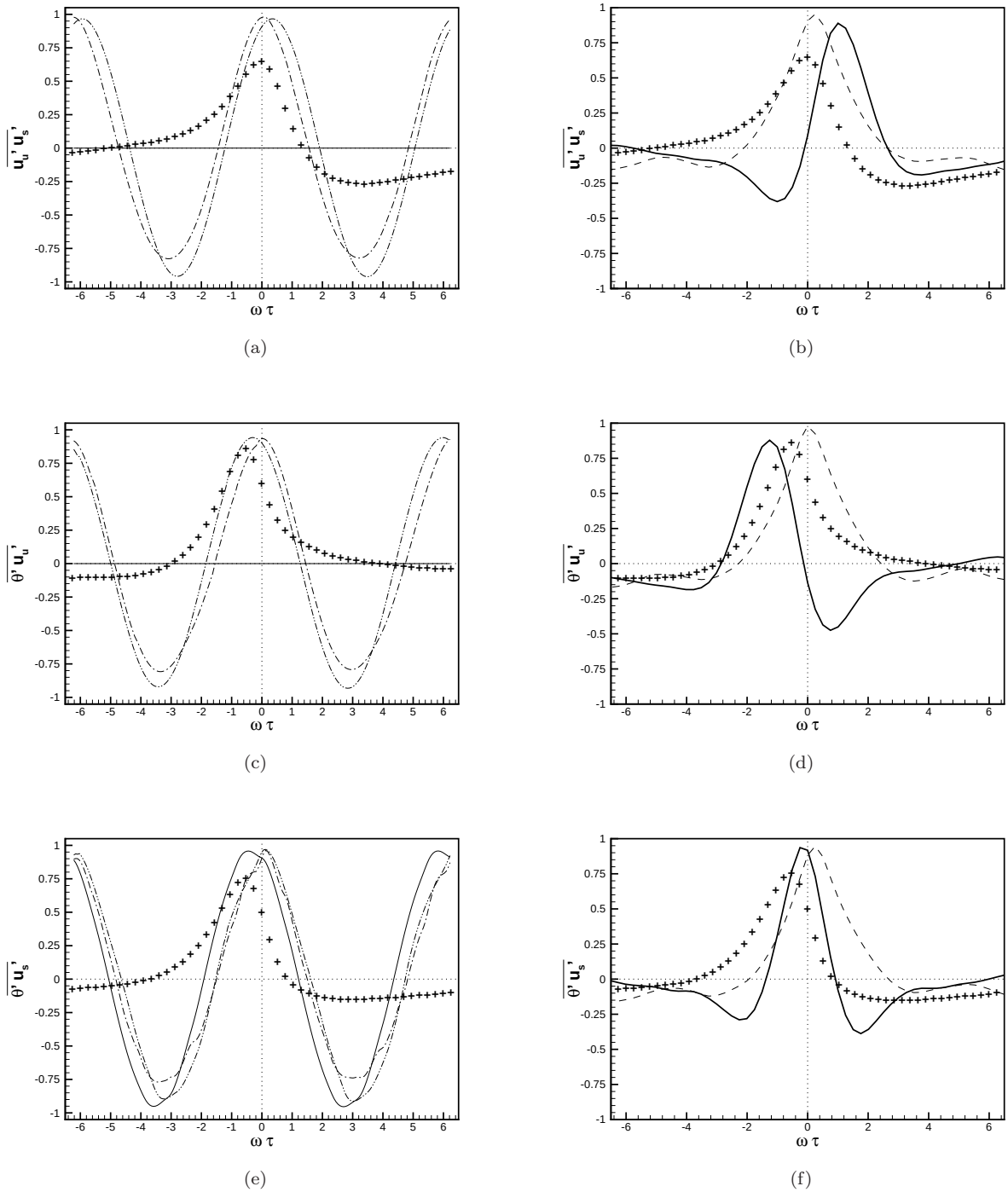

Figure 9. Correlation coefficients of (a,b) $\overline{u'_u u'_s}$, (c,d) $\overline{\theta' u'_u}$ where θ is the shock-strength and (e,f) $\overline{\theta' u'_s}$ for entropy wave (Thin solid), right moving acoustic wave (DashDotDot), left moving acoustic wave (DashDot), broadband of right moving acoustic waves (Thick Solid), broadband of left moving acoustic waves (Dashed) and shock/turbulence interaction (Symbols).

shock speed with shock location shown in figure 8 goes to 0 for $\omega\tau = 0$. The match between DNS case and the broadband cases is quite remarkable as seen in figure 8 (b), especially for the broadband left moving acoustic case. Also, this correlation is antisymmetric for all the cases about the $\omega\tau = 0$ axis.

It is often assumed that the shock unsteadiness in a canonical shock-turbulence interaction is a response to the incoming fluctuations in the upstream flow. The shock speed can therefore be expected to be correlated to the upstream velocity fluctuations in the streamwise direction.

The correlation between the instantaneous values of upstream velocity fluctuations and the shock speed for one dimensional single mode cases is 1 as seen in figure 9(a) and the correlation shows a periodic variation with changes in the time lag τ. This is in agreement with LIA predictions. Note that the case with a pure entropy mode upstream of the shock has zero velocity fluctuations, and hence a zero correlation for all τ.

The DNS data of full shock/turbulence interaction has a peak correlation coefficient of about 0.65 at zero time lag, but the variation with τ is not sinusoidal, as expected. This is true for the broadband one-dimensional case with left-moving acoustic waves. The correlation reaches a maximum of 0.9 in this case, and falls off to negative values for larger time lags. The interaction with right moving broadband acoustic waves shows a different trend. Unlike the other cases in in this flow, the instantaneous upstream velocity and the shock speed are not correlated ($\overline{u'_u u_s}$ close to 0 for $\tau = 0$). The correlation attains a peak positive value close to 0.9 at a time lag of $\omega\tau = 1$ and a peak negative value for $\omega\tau = -1$.

Next, we plot the correlation between shock strength and upstream velocity fluctuation normal to the shock in figures 9(c) and 9(d). The correlation coefficient in the single mode cases and the left-moving acoustic broadband case show a pattern similar to that described above. They attain peak values close to one at zero time lag, which means a higher velocity fluctuation upstream of the shock sees a stronger shock and vice-versa. The single mode interactions, once again, yield sinusoidal variation of the correlation coefficient, whereas the broadband case appears to be symmetric about the $\tau = 0$ axis.

For DNS, the peak correlation takes a value of about 0.8, but shifts to a negative value of the time lag. The broadband acoustic case with right-moving waves upstream of the shock, like earlier, yields zero correlation between the instantaneous shock strength and the upstream velocity fluctuations. The maximum and minimum in the correlation coefficient occur at $\omega\tau = -2$ and $\omega\tau = 1$ respectively. As a result, the pattern looks opposite to that of the $\overline{u'_u u'_s}$ data for the same case in figure 9(b).

Finally, we plot the correlation between the instantaneous shock strength and the shock speed in figures 9(e) and 9(f). The DNS case also has a high $\overline{\theta' u'_s}$ correlation (around 0.75) at $\omega\tau = -1$. This indicates that positive shock speed is followed by a stronger shock. So, the shock is going to be stronger if it is pushed back than if it is pushed forward. This is also shown by Larsson *et al.*[4] All the one dimensional interactions peak closer to $\tau = 0$.

This suggests that there is a qualitative difference between one dimensional and three dimensional shock-turbulence interaction cases in the physical mechanisms that govern shock strength. Also, shock strength is directly connected to the creation of shock holes (shock holes occur when shock strength goes to zero). This is consistent with the earlier finding (in section 3) that one dimensional interactions seem qualitatively different from three dimensional interactions in terms of creation of shock holes.

V. Conclusion

In this paper we study one-dimensional interactions between a shock wave and incoming disturbances. The objective is to gain insight into the one-dimensional physics of shock/turbulence interaction. Specifically, we investigate if one dimensional simulations can qualitatively and quantitatively reproduce the shock dynamics observed in three dimensional cases. Most importantly, can we break the shock using high intensity one-dimensional waves and create shock-holes that have been observed in shock-turbulence interactions.

Inviscid simulations are performed for a Mach 1.5 shock with upstream acoustic and entropy waves; both single mode and broadband acoustic disturbances are considered. It is found that the shock oscillations increase in amplitude with an increase in the upstream fluctuation level. Even at the highest intensity of the incoming wave, the shock remains intact and no shock holes are observed. The upstream intensities exceed the criterion for shock holes proposed for three-dimensional turbulence, which suggests that shock holes cannot be replicated in one-dimensional simulations.

Next, we compare the shock statistics obtained from one-dimensional simulations with those in three-dimensional DNS of shock-turbulence interaction. We compute correlations between shock speed, location, strength and upstream velocity fluctuations, as a function of a normalized time lag, for different types of

incoming disturbances. The single mode computations yield correlations coefficients that are sinusoidal with a peak value of 1. On the other hand, correlations for the broadband acoustic cases are asymmetric, akin to the DNS data. It is found that the correlation between shock strength and shock speed shows a systematic difference between the one-dimensional simulations and the three-dimensional DNS. This bolsters the argument that there is a qualitative difference between one dimensional and three dimensional interactions in terms of mechanisms that govern shock strength and create shock holes.

Acknowledgments

A portion of the computer time was provided by the NPSF PARAM YUVA II facility in C-DAC, Pune, India.

References

[1]Hesselink, L. and Sturtevant, B., "Propagation of weak shocks through a random medium," *J. Fluid Mech.*, Vol. 196, 1988, pp. 513–553.

[2]Lee, S., Lele, S. K., and Moin, P., "Direct numerical simulation of isotropic turbulence interacting with a weak shock wave," *J. Fluid Mech.*, Vol. 251, 1993, pp. 533–562.

[3]Larsson, J. and Lele, S. K., "Direct numerical simulation of canonical shock/turbulence interaction," *Phys. Fluids*, Vol. 21, No. 12, 2009, 126101.

[4]Larsson, J., Bermejo-Moreno, I., and Lele, S. K., "Reynolds- and Mach-number effects in canonical shock-turbulence interaction," *J. Fluid Mech.*, Vol. 717, 2013, pp. 293–321.

[5]Donzis, D. A., "Shock structure in shock-turbulence interactions," *Phys. Fluids*, 2012, pp. 126101.

[6]Zank, G. P., Zhou, Y., Matthaeus, W. H., and Rice, W. K. M., "The interaction of turbulence with shock waves: A basic model," *Phys. Fluids*, Vol. 14, No. 11, 2002, pp. 3766–3774.

[7]Larsson, J., "Effect of shock-capturing errors on turbulence statistics," *AIAA J.*, Vol. 48, No. 7, 2010, pp. 1554–1557.

[8]Kovásznay, L. S. G., "Turbulence in supersonic flow," *J. Aero. Sci.*, Vol. 20, No. 10, 1953, pp. 219–237.

[9]Mahesh, K., Moin, P., and Lele, S. K., "The interaction of a shock wave with a turbulent shear flow," Tf-69, Thermosciences Division, Department of Mechanical Engineering, Stanford University, Stanford, California, June 1996.